Fully computable a posteriori error estimates for the primal hybrid variational formulation of Poisson's equation

Victor B. Oliari[1], Paulo Rafael Bösing[2], Denise de Siqueira[3], Philippe R. B. Devloo[1]

[1]*Dept. of Civil Engineering, State University of Campinas (UNICAMP)*
Saturnino de Brito street 224, 13083-889, Campinas/SP, Brazil
oliari.victor@gmail.com, phil@fec.unicamp.br
[2]*Dept. of Mathematics, Federal University of Fronteira Sul (UFFS)*
High road SC 484 - Km 02, 89815-899, Chapecó/SC, Brazil
paulo.bosing@uffs.edu.br
[3]*Dept. of Mathematics, Federal University of Technology – Paraná (UTFPR-CT)*
Sete de Setembro avenue, 80230-901, Curitiba/Paraná, Brazil
denisesiqueira@utfpr.edu.br

Abstract. We present a new fully computable a posteriori error estimates for the primal hybrid formulation applied to Poisson's problem. The estimates are based on the reconstruction of a continuous potential field and an equilibrated flux, which are computed using the potential and Lagrange multipliers solutions. The potential reconstruction is the result of orthogonally projecting the potential solution onto a function over the mesh skeleton, smoothing this function into a continuous trace, and solving local pure Dirchlet problems. This procedure for reconstructing the potential were used to develop error estimates for the mixed formulation in [1, 2]. The equilibrated flux is obtained from solving local mixed problems using Lagrange multipliers at a pure Neumann boundary condition. This technique is similar to the flux recovery strategy based on the Arnold–Boffi–Falk spaces described in [3], but for the divergent compatible pair of spaces described in [4]. An adaptive refinement strategy is developed, and numerical results illustrate the efficiency of the error estimates.

Keywords: FEM, Primal hybrid, Adaptive refinement, A posteriori error estimates

1 Introduction

A posteriori error estimates provide an upper bound for the approximation error using the solution of the finite element formulation. In the literature, a posteriori estimates can be found for H^1-conforming [5] and nonconforming [2] methods. We propose new a posteriori error estimates applied to the primal hybrid formulation of Poisson's equation. The estimates are based on the Generalized Prager–Synge (GPS) identity [6], which extends Prager-Synge identity to nonconforming methods, and on the reconstruction of a continuous potential and equilibrated flux fields. The mathematical development relies on Helmholtz decomposition of the error.

The reconstruction of the potential field is based on an element-wise L^2 orthogonal projection of the numerical solution, and the field continuity is ensured by using a continuous function defined on the mesh skeleton as a Dirchlet boundary condition. A similar reconstruction method is described in [2], but the primal hybrid approximation space for the potential variable requires no uplifting. An equilibrated flux is built by solving element-wise problems for which the Lagrange multipliers numerical solution is used as a boundary condition. A similar technique for reconstructing the flux variable is described in [3].

An adaptive refinement strategy is proposed based on the error estimates and a mesh smoothing procedure. The quality of the error estimates is evaluated for a numerical problem with an irregular solution.

2 Notations and preliminaries

Consider the model problem of finding a potential u defined over an open convex domain $\Omega \in \mathbb{R}^2$. The domain is bounded by the polygonal boundaries $\partial\Omega_D$ and $\partial\Omega_N$, and the following relations

$$\left\{\begin{array}{rcll} \nabla\cdot(-\mathbf{K}\nabla u) & = & f, & \text{in } \Omega \\ u & = & g_N, & \text{on } \partial\Omega_D \\ -\boldsymbol{K}\nabla u\cdot\boldsymbol{n} & = & g_D, & \text{on } \partial\Omega_N \end{array}\right. , \tag{1}$$

hold. Where $\boldsymbol{K}$ is a positive definite second-order tensor and $\boldsymbol{n}$ is the normal unit vector pointing outwards of Ω.

Let $L^2(\Omega) = \{f \in \mathbb{R} | \int_\Omega f^2 < \infty\}$ be the space of square integrable functions, which is equipped with the inner product $(v_1, v_2) = \int_\Omega v_1\, v_2\, d\Omega$ for any $v_1, v_2 \in L^2(\Omega)$ and the norm $\|f\| = \sqrt{(f,f)}$. Let $H^1(\Omega) = \{v \in L^2(\Omega) | D^1 v \in L^2(\Omega)\}$ be the space of once differentiable functions, which is equipped with the semi-norm $|v|_1 = \|D^1 v\|$ and the norm $\|v\|_1 = \|v\| + |v|_1$. Set a subspace of admissible functions $H^1_\xi(\Omega) = \{v \in H^1(\Omega) \text{ s. t. } v|_{\partial\Omega_D} = \xi\}$. A variational approximation for the model problem eq. (1) can be developed by supposing that the solution belongs to a sufficiently smooth space, by multiplying both sides by a test function, and by applying the chain rule. The standard variational formulation for the model problem consists of finding $u \in H^1(\Omega)$ satisfying

$$(\boldsymbol{K}\nabla u, \nabla v) = (f, v) + \langle g_N, v\rangle_{\partial\Omega_N}, \qquad \forall v \in H^1_0(\Omega). \tag{2}$$

Consider partitions $\mathcal{T}_h = \{K\}$ of the domain Ω comprising open, convex, piecewise disjoint and juxtaposed quadrilateral elements K, and let $\mathbb{T} = \{\mathcal{T}_h\}$ be a set containing some of these partitions. The set of all edges $E \in \partial K$ for all $K \in \mathcal{T}_h$ is the mesh skeleton $\mathcal{E}_h$, which can be decomposed into internal $\mathring{\mathcal{E}}_h$ and boundary $\mathcal{E}_{h,\partial}$ skeletons. The maximum element diameter within each partition is given by $h = \max_{K\in\mathcal{T}_h} h_K$.

The standard formulation can be posed in terms of finite elements K, resulting into a continuous potential field u_h. The primal hybrid [7] variational formulation for the model problem can be developed by breaking the inter-element continuity of the solution u_h and by imposing a Lagrange multiplier $\lambda_h(s)$, $s \in \mathcal{E}_h$ representing the normal component of the flux $\lambda_h \approx -\boldsymbol{K}\nabla u_h \cdot \boldsymbol{n}^K$ at the elements interfaces. The field $\boldsymbol{n}^K$ corresponds to the unit normal vector points outwards of the element K. Before stating the primal hybrid formulation, additional definitions are required.

Let $H^1(\mathcal{T}_h) = \{v_h \in L^2(\Omega)\,|\, v_h|_K \in H^1(\mathcal{T}_h), \forall K \in \mathcal{T}_h\}$ be the broken Hilbert space and consider the set of admissible functions $H^1_{\xi_h}(\mathcal{T}_h) = \{v_h \in H^1(\mathcal{T}_h) | -\boldsymbol{K}\nabla v_h|_{\partial\Omega_N}\cdot\boldsymbol{n}^K = \xi_h\}$. The space of vector functions with square-integrable weak divergences is denoted by $\boldsymbol{H}(\mathrm{div};\Omega) = \{\boldsymbol{v} \in [\boldsymbol{L}^2(\Omega)]^2\,|\,\nabla\cdot\boldsymbol{v} \in L^2(\Omega)\}$ and a subset of admissible vector functions by $\boldsymbol{H}_\xi(\mathrm{div};\Omega) = \{\boldsymbol{v} \in \boldsymbol{H}(\mathrm{div};\Omega) \text{ s. t. } \boldsymbol{v}\cdot\boldsymbol{n}|_{\partial\Omega_N} = \xi\}$. The space of Lagrange multipliers $\Lambda(\mathcal{E}_h)$ represents the trace of functions in $\boldsymbol{H}(\mathrm{div};\Omega)$ over the skeleton $\mathcal{E}_h$, and the subspace of admissible functions $\Lambda_\xi(\mathcal{E}_h)$ corresponds to the trace of functions in $\boldsymbol{H}_\xi(\mathrm{div};\Omega)$.

Let $\hat{\mathcal{P}}_n(s) : \mathbb{R} \to \mathbb{R}$ be a space of polynomials of order n defined over a reference line segment $\hat{E}$. The space of bi-dimensional polynomials is denoted by $\hat{\mathcal{Q}}_{n_1,n_2}(\boldsymbol{x}) : \{\boldsymbol{x} \in \mathbb{R}^2\,|\,\boldsymbol{v}_h \in \hat{\mathcal{Q}}_{n_1,n_2}\,|\,\boldsymbol{v}_h\cdot\hat{\boldsymbol{e}}_i \in \mathcal{P}_{n_i},\, i = \{1,2\}\}$ or simply by $\hat{\mathcal{Q}}_n$ when $n_1 = n_2$, and are defined over a reference quadrilateral element $\hat{K}$. The coordinate transformation from a reference $\hat{(\cdot)}$ to a deformed $(\cdot)$ configuration can be achieved with an appropriate mapping. Now the finite element spaces can be set. Consider the spaces $U^n_h(\mathcal{T}_h) = \{v_h \in L^2(\Omega) \text{ s. t. } v_h|_K \in \mathcal{Q}_n(K)\}$, $V^n_h(\Omega) = \{v_h \in H^1(\Omega) \text{ s. t. } v_h|_K \in \mathcal{Q}_n(K)\}$ and $\Lambda^n_h(\mathcal{E}_h) = \{\mu_h \in \Lambda(\mathcal{E}_h) \text{ s. t. } \mu_h|_E \in \mathcal{P}_n\}$, and the corresponding subspaces $U^n_{h,\xi}(\mathcal{T}_h) \subset H^1_\xi(\mathcal{T}_h)$, $V^n_{h,\xi}(\Omega) \subset H^1_\xi(\Omega)$ and $\Lambda^n_{h,\xi}(\mathcal{E}_h) \subset \Lambda_\xi(\mathcal{E}_h)$.

The primal hybrid finite element formulation consists of finding $(\lambda_h, u_h) \in \Lambda^1_{h,g_{h,N}}(\mathcal{E}_h) \times U^3_h(\mathcal{T}_h)$ for all $(\mu_h, v_h) \in \Lambda^1_{h,0}(\mathcal{E}_h) \times U^3_h(\mathcal{T}_h)$, such that

$$\begin{aligned} \sum_{K\in\mathcal{T}_h}\left[(\boldsymbol{K}\nabla u_h, \nabla v_h)_K + \langle\,\lambda_h,\, v_h\rangle_{\partial K}\right] &= \sum_{K\in\mathcal{T}_h}(f_h,\, v_h)_K \\ \sum_{K\in\mathcal{T}_h}\langle u_h, \mu_h\rangle_{\partial K} &= \sum_{K\in\mathcal{T}_h}\langle g_{h,N}, \mu_h\rangle_{\partial K\cap\partial\Omega_D}, \end{aligned} \tag{3}$$

where $g_{h,N}$, $g_{h,D}$ and f_h are the local L^2-orthogonal projections of functions g_N, g_D and f over their respective

supports and with respect to the corresponding finite element spaces. The polynomial basis are constructed using hierarchical shape functions. A systematic procedure for constructing hierarchical basis can be found in [8].

A finite element space for vector functions is also required. The choice $\hat{\boldsymbol{M}}_h^{k,n} = \{\boldsymbol{v} \in \mathcal{Q}_{k+n+1,k} \times \mathcal{Q}_{k,k+n+1}\}$ has some interesting properties. For a function $\hat{\boldsymbol{v}} \in \hat{\boldsymbol{M}}_h^{k,n}(\hat{K})$, its divergent belongs to to a complete polynomial space $\nabla \cdot \hat{\boldsymbol{v}} \in \hat{U}_h^{k+n}(\hat{K})$ and its normal component over an element boundary is a polynomial of order k, $\hat{\boldsymbol{v}} \cdot \hat{\boldsymbol{n}}^K \in \Lambda_h^k(\hat{\mathcal{E}}_h)$. The parametric space $\hat{\boldsymbol{M}}_h^{k,n}$ can be mapped to the deformed configuration $\boldsymbol{M}_h^{k,n}$ through Piola's transformation. The definition of the finite element space of admissible functions $\boldsymbol{M}_{h,\xi}^{k,n}(\Omega) \subset \boldsymbol{H}_\xi(\mathrm{div};\Omega)$ can be easily deducted. Therefore, the family of space pairs $\boldsymbol{M}_h^{k,n} \times U_h^{k+n}(\mathcal{T}_h)$ fulfills De Rham's condition and coincides with the classical Raviart-Thomas space RT_k for $n = 0$. More details about constructing such spaces can be found in [9].

3 A posteriori error estimates

The development of the a posteriori error estimates for the primal hybrid formulation is based on the Generalized Prager Synge Inequality (GPS) [6]. Let $\boldsymbol{\Sigma}_f(\Omega) = \{\boldsymbol{\tau} \in \boldsymbol{H}(\mathrm{div};\Omega) \,|\, \nabla \cdot \boldsymbol{\tau} = f, \text{ and } \boldsymbol{\tau} \cdot \boldsymbol{n}|_{\partial\Omega_N} = g_N\}$ be the space of equilibrated fluxes. The solution of eq. (1) $u \in H^1_{g_D}(\Omega)$ is related to a piecewise continuous field $w \in H^1(\mathcal{T}_h)$, an equilibrated flux $\boldsymbol{\tau} \in \boldsymbol{\Sigma}_f(\Omega)$ and a continuous field $v \in H^1_{g_D}(\Omega)$ through Theorem 1.

Theorem 1. *Let $u \in H^1_{g_D}(\Omega)$ be the solution of eq.* (1)*. In two dimensions, for all $w \in H^1(\mathcal{T}_h)$, we have*

$$\|\boldsymbol{K}^{1/2}\nabla(u-w)\|^2 = \inf_{\boldsymbol{\tau}\in\boldsymbol{\Sigma}_f(\Omega)} \|\boldsymbol{K}^{-1/2}\boldsymbol{\tau} + \boldsymbol{K}^{1/2}\nabla w\|^2 + \inf_{v\in H^1_{g_D}(\Omega)} \|\boldsymbol{K}^{1/2}\nabla(v-w)\|^2.$$

The error estimates are derived by applying Helmholtz decomposition, by using the GPS identity described in Theorem 1, and by selecting appropriate reconstruction fields. Let $\boldsymbol{t} \in \boldsymbol{M}_h^{1,2} \subset \boldsymbol{\Sigma}_f(\Omega)$ and $s_h \in V^3_{h,g_{h,D}}(\Omega) \subset H^1_{g_{h,D}}(\Omega)$ be a reconstructed flux and potential, respectively, which are built from the solutions of eq. (3). A superior bound for the error is described in Theorem 2.

Theorem 2. *Let u be the solution of eq.* (2)*, and $u_h \in U_h^3(\mathcal{T}_h)$ be the solution of the primal hybrid approximation* (3)*. Let $s_h \in V^3_{h,g_{h,D}}(\Omega)$ represent the potential reconstruction, and let $\boldsymbol{t}_h \in \boldsymbol{M}_h^{1,2}$ be the reconstructed flux. The following upper bound holds:*

$$\|\boldsymbol{K}^{1/2}\nabla(u-u_h)\|^2 \leq \left[\left(\sum_{E\in\partial\Omega_N} \eta_{E,B}^2\right)^{1/2} + \left(\sum_{K\in\mathcal{T}_h} (\eta_{K,R}+\eta_{K,f})^2\right)^{1/2}\right]^2 + \sum_{K\in\mathcal{T}_h} \eta_{K,p}^2,$$

where

$$\eta_{K,R} = \frac{C_P^{1/2} h_K}{C_{\boldsymbol{K},K}^{1/2}} \|f - \nabla\cdot\boldsymbol{t}_h\|_K, \quad \eta_{K,f} = \|\boldsymbol{K}^{-1/2}(\boldsymbol{t}_h + \boldsymbol{K}\nabla u_h)\|_K,$$

$$\eta_{K,p} = \|\boldsymbol{K}^{1/2}\nabla(s_h - u_h)\|_K \quad \textit{and} \quad \eta_{E,B} = \xi^{1/2}(\boldsymbol{K}, C_P, C_t) h_K^{1/2} \|g - g_h\|_E.$$

where $C_P = 1/\pi^2$ (see [10] and references therein) is the constant from the Poincaré inequality, $C_{\boldsymbol{K},K}$ is the smallest eigenvalue of $\boldsymbol{K}$ on element K, C_t is the trace inequality constant and

$$\xi(\boldsymbol{K}, C_P, C_t) := C_t \left(\frac{C_P}{C_{\boldsymbol{K},K}^{1/2}} + \frac{C_P^{1/2}}{C_{\boldsymbol{K},K}^{3/4}}\right).$$

Potential reconstruction: The solution u_h of the primal hybrid problem (eq. (3)) is in general discontinuous along element interfaces, and the error estimates described in Theorem 2 require a continuous potential field. Let $s_h^K \in V_h^3(K)$ be the potential field satisfying the following element-wise problem,

$$\begin{aligned} (\boldsymbol{K}\nabla s_h^K, \nabla v_h)_K &= (\boldsymbol{K}\nabla u_h^K, \nabla v_h)_K, \\ s_h^K &= \gamma_h|_{\partial K} \quad \text{on} \quad \partial K. \end{aligned} \tag{4}$$

for all $v_h \in V^3_{h,0}(K)$, where $\gamma_h \in \Pi_{E\in\mathcal{E}_h}\mathcal{P}_3(E)$ is a continuous function built from piece-wise polynomials on each mesh skeleton's edge, and $\Pi(.)$ is defined in the sense of the Cartesian product. The continuous field $s_h \in V^3_{h,g_{h,D}}(\Omega)$ follows from $s_h|_K = s_h^K$.

The construction of the continuous function γ_h is based on the work of [2]. Let $\gamma_h^{(0)}$ be a function with support over the mesh skeleton, computed as follows.

$$\gamma_h^{(0)}|_E = \begin{cases} \displaystyle\int_E \frac{\omega^+ u_h^+ + \omega^- u_h^-}{\omega^+ + \omega^-} - \gamma_h^{(0)}\, ds = 0 & \text{for } E \in \mathring{\mathcal{E}}_h; \\ \gamma_h^{(0)} = u_h & \text{for } E \in \mathcal{E}_{h,\partial}, \end{cases} \tag{5}$$

where the $\omega^{+/-}$ corresponds to the maximum eigenvalue of tensor $\boldsymbol{K}$ for element $K^{+/-}$.

Function $\gamma_h^{(0)}$ is discontinuous at the mesh skeleton nodes. The nodal values of $\gamma_h^{(0)}$ are updated by computing a weighted nodal average, resulting in the continuous field γ_h. Figure 1 illustrates the difference between the solution u_h and the reconstructed potential s_h.

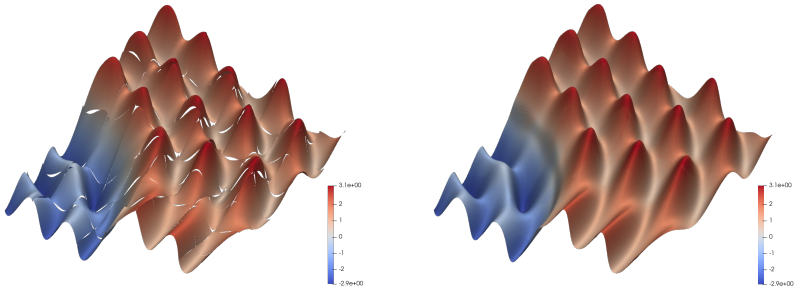

(a) u_h (b) s_h

Figure 1. Solution u_h (left) and reconstructed potential s_h (right) and .

Flux reconstruction: An element-wise equilibrated flux $\boldsymbol{t}_h^K \in \boldsymbol{\Sigma}_f(K)$ follows from the problem: find $(\boldsymbol{t}_h^K, p_h^K) \in \mathbf{M}_{h,\lambda_h}^{1,3}(K) \times V_h^3(K)$ satisfying

$$\begin{aligned} (\boldsymbol{K}^{-1}\boldsymbol{t}_h^K, \boldsymbol{v})_K - (p_h^K, \nabla\cdot\boldsymbol{v})_K &= 0\,, \\ -(\nabla\cdot\boldsymbol{t}_h^K, w)_K &= -(f, w)_K\,, \end{aligned} \tag{6}$$

for all $(\boldsymbol{v}, w) \in \mathbf{M}_{h,0}^{1,3}(K) \times V_h^3(K)$. The equilibrated flux $\boldsymbol{t}_h \in \boldsymbol{\Sigma}_f(\Omega)$ is obtained by restricting its value to the element-wise solutions, $\boldsymbol{t}_h|_K = \boldsymbol{t}_h^K$.

4 Adaptive h-refinement strategy

We propose an adaptive h-refinement strategy based on the error estimates. A mesh $\mathcal{T}_h^{(0)}$ is chosen over which the fields $u_h^{(0)}, \lambda_h^{(0)}$ are computed through eq. (3). The error estimates are computed according to Theorem 2, and the following element-wise error estimator is calculated

$$\left[\eta_{estim}^K\right]^2 = \left[\eta_{E_N,B} + \eta_{K,R} + \eta_{K,f}\right]^2 + \eta_{K,p}^2.$$

where $E_N = \partial K \cap \partial\Omega_N$. The maximum error per element $\eta_{max}^K = \max_{K\in\mathcal{E}_h} \eta_{estim}^K$ is computed and elements for which $\eta_{estim}^K > \tau\eta_{max}^K$ are marked for refinement. This procedure is illustrated in Figure 2.

After refining the elements with expressive errors, two mesh smoothing procedure are used. Elements with two-levels finer neighbours and elements encircled with at least three finer neighbours are also refined. The mesh smoothing procedure is illustrated in Figure 3. The adaptive strategy is repeated until a prescribed number of refinement steps is reached.

5 Numerical results

Problem with contrasting tensors $\boldsymbol{K}$: To illustrate the efficiency of the error estimates, the proposed indexes are evaluated over a problem with contrasting permeability tensors. The problem consists of finding u satisfying

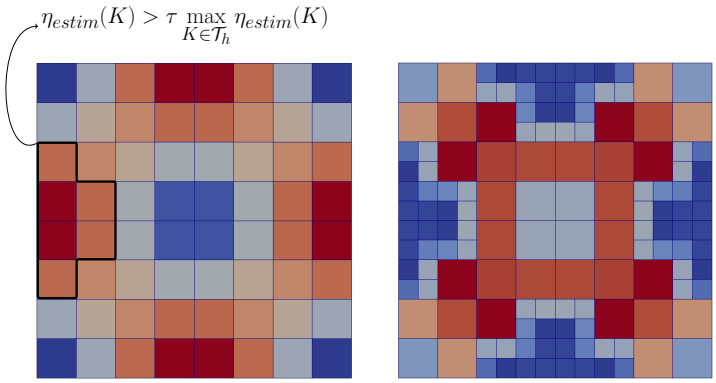

Figure 2. Marking elements for adaptive refinement (left) and mesh after refinement (right).

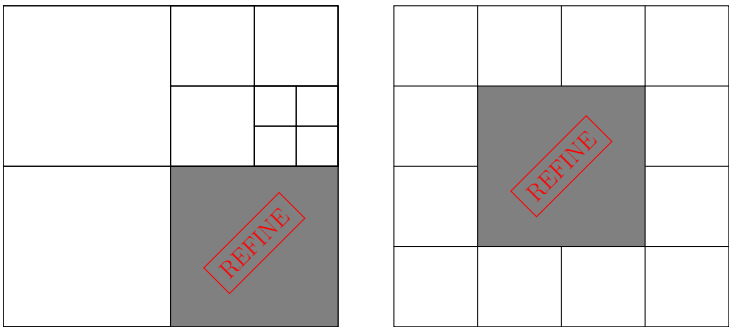

Figure 3. Refinement of elements with a two-levels finer neighbour (left) and elements encircled by finer elements (right).

eq. (1) over $\Omega = [-1, 1] \times [-1, 1]$ with

$$u = g_D = r^{\lambda} \left\{ \alpha \cos\left[\lambda \arctan\left(\theta\right)\right] + \beta \sin\left[\lambda \arctan\left(\theta\right)\right] \right\}$$

over $\partial\Omega = \partial\Omega_D$, where r is the Euclidean distance from the origin, and the coefficients α, β and λ are found by solving Steklov's problem for a permeability tensor $\boldsymbol{K} = 5I$ on odd quadrants and $\boldsymbol{K} = I$ on even quadrants. Figure 4 illustrates this problem solution and its gradient.

u $\qquad\qquad$ $\|\boldsymbol{K}\nabla u\|$

Figure 4. Problem with contrasting tensors $\boldsymbol{K}$: the solution u on the left and the magnitude of the gradient $\|\boldsymbol{K}\nabla u\|$. on the right

A family of partitions $\mathbb{T}_u = \{\mathcal{T}_h\}$ with $h \in \{1, 1/2, 1/4, 1/8, 1/16, 1/32\}$ of uniformly refined meshes is selected. The estimated η_{estim} and exact errors η_{exact} for this family of partitions is shown in Figure The convergence graph of the estimated and exact errors is documented in Figure 5. The estimated error converges in h at the same rate as the exact error, showing an an asymptotically exact convergence pattern.

A second family of partitions $\mathbb{T}_a = \{\mathcal{T}_h^{(i)}\}$ is built from applying nineteen adaptive refinement steps to an

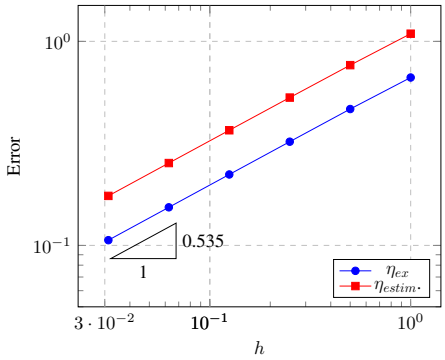

Figure 5. Problem with contrasting tensors $\boldsymbol{K}$: Histories of convergence of the exact η_{ex} and estimated errors η_{estim}.

initial mesh $\mathcal{T}_h^{(0)} = \mathcal{T}_{h=1}$ and a threshold $\tau = 0.60$. On the left side of Figure 6, the estimated errors for the adaptive and uniform refinement strategies are shown. For the adaptive strategy, the estimated errors are up to two orders of magnitude lower than for the uniform refinement. The effectivity index describes the accuracy of the error estimates, and are shown on the right side of the figure. The indexes for the adaptive strategy are closer to one, exhibiting closer estimates to the exact errors.

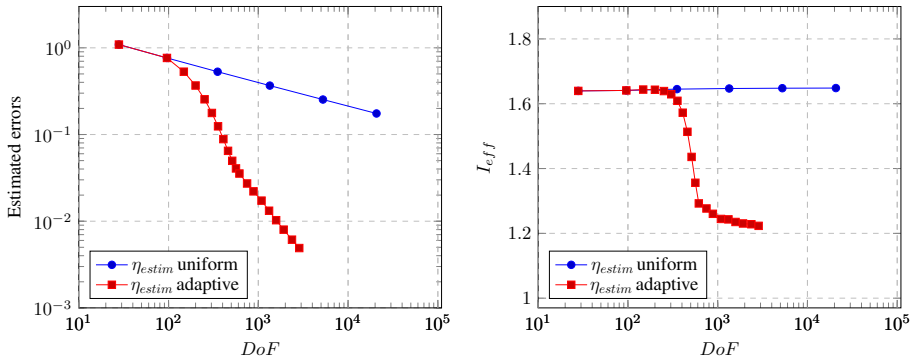

Figure 6. Problem with contrasting tensors $\boldsymbol{K}$: On the left, the estimated errors for the uniform and adaptive strategies. On the right, the effectivity index for each family of partitions.

The developed estimates also enable an assessment of the error per finite element, as shown in Figure 7. The figure on left-most side corresponds to the adaptive refinement step 7, followed by steps 14 and 19, respectively. It is clear that the strategy leads to smaller elements in the direction of the discontinuity, as intended.

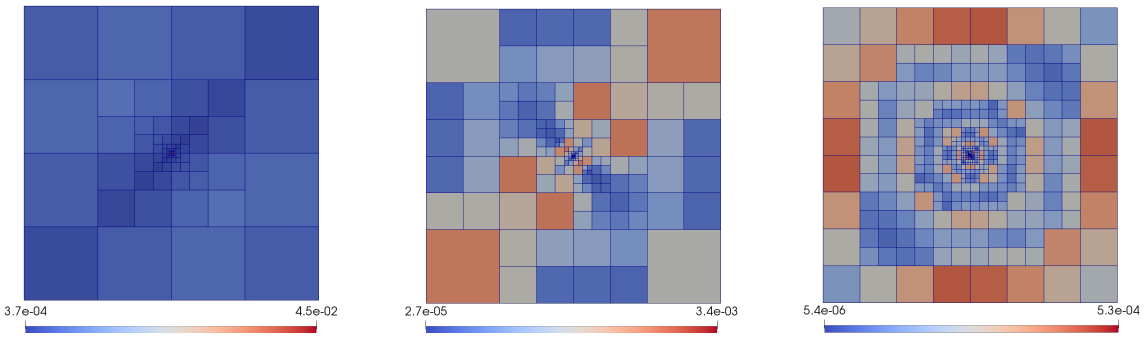

step $i = 7$ step $i = 14$ step $i = 19$

Figure 7. Problem with contrasting tensors $\boldsymbol{K}$: Estimated error per element for the three adaptive steps $i \in \{8, 13, 18\}$.

6 Conclusions

This paper presents a posteriori error estimates for the finite element primal hybrid formulation of Poisson's equation. The estimates are based on the reconstruction of a continuous potential field and an equilibrated flux. An adaptive h-refinement strategy based on the error estimates and a mesh smoothing procedure was proposed. The quality of the estimate results and the refinement strategy was numerically verified over a problem with contrasting permeability tensors, for which the gradient of the solution is irregular at the origin. The adaptive refinement strategy showed errors up to two orders of magnitude lower than for the uniform refinement.

Acknowledgements. We gratefully acknowledge the support of EPIC – Energy Production Innovation Center, hosted by the University of Campinas (UNICAMP) and sponsored by Equinor Brazil and FAPESP – Sao Paulo Research Foundation (process 2017/15736-3). We acknowledge the support of ANP (Brazil National Oil, Natural Gas and Biofuels Agency) through the R&D levy regulation. Acknowledgments are extended to the Center for Petroleum Studies (CEPETRO), School of Mechanical Engineering (FEM) and School of Civil Engineering (FEC).

Authorship statement. The authors hereby confirm that they are the sole liable persons responsible for the authorship of this work, and that all material that has been herein included as part of the present paper is either the property (and authorship) of the authors, or has the permission of the owners to be included here.

References

[1] G. A. Batistela, de D. Siqueira, P. R. Devloo, and S. M. Gomes. A posteriori error estimator for a multiscale hybrid mixed method for darcy's flows. *International Journal for Numerical Methods in Engineering*, vol. 123, n. 24, pp. 6052–6078, 2022.

[2] M. Ainsworth and X. Ma. Non-uniform order mixed fem approximation: implementation, post-processing, computable error bound and adaptivity. *Journal of Computational Physics*, vol. 231, n. 2, pp. 436–453, 2012.

[3] M. R. Correa and G. Taraschi. Optimal h (div) flux approximations from the primal hybrid finite element method on quadrilateral meshes. *Computer Methods in Applied Mechanics and Engineering*, vol. 400, pp. 115539, 2022.

[4] P. Remy Bernard Devloo, O. Durán, A. Monteiro Farias, and S. Maria Gomes. H (div) finite elements based on nonaffine meshes for 3d mixed formulations of flow problems with arbitrary high order accuracy of the divergence of the flux. *International Journal for Numerical Methods in Engineering*, vol. 121, n. 13, pp. 2896–2915, 2020.

[5] M. Vohralík. Guaranteed and fully robust a posteriori error estimates for conforming discretizations of diffusion problems with discontinuous coefficients. *Journal of Scientific Computing*, vol. 46, n. 3, pp. 397–438, 2011.

[6] Z. Cai, C. He, and S. Zhang. Generalized prager–synge identity and robust equilibrated error estimators for discontinuous elements. *Journal of Computational and Applied Mathematics*, vol. 398, pp. 113673, 2021.

[7] P. A. Raviart and J. M. Thomas. Primal hybrid finite element methods for 2nd order elliptic equations. *Mathematics of Computation*, vol. 31, pp. 391–413, 1977.

[8] P. R. B. Devloo, C. M. A. A. Bravo, and E. C. Rylo. Systematic and generic construction of shape functions for p-adaptive meshes of multidimensional finite elements. *Computer Methods in Applied Mechanics and Engineering*, vol. 198, n. 21-26, pp. 1716–1725, 2009.

[9] D. A. Castro, P. R. Devloo, A. M. Farias, S. M. Gomes, de D. Siqueira, and O. Durán. Three dimensional hierarchical mixed finite element approximations with enhanced primal variable accuracy. *Computer Methods in Applied Mechanics and Engineering*, vol. 306, pp. 479–502, 2016.

[10] M. Vohralík. Unified primal formulation-based a priori and a posteriori error analysis of mixed finite element methods. *Math. Comput.*, vol. 79(272), pp. 2001–2032, 2010.